Discovery of blue singlet exciton fission molecules via a high-throughput virtual screening and experimental approach

The Journal of Chemical Physics

Discovery of blue singlet exciton fission molecules via a high-throughput virtual screening and experimental approach

Cite as: J. Chem. Phys. **151**, 121102 (2019); https://doi.org/10.1063/1.5114789
Submitted: 11 June 2019 . Accepted: 28 August 2019 . Published Online: 24 September 2019

Collin F. Perkinson, Daniel P. Tabor, Markus Einzinger, Dennis Sheberla, Hendrik Utzat, Ting-An Lin, Daniel N. Congreve, Moungi G. Bawendi, Alán Aspuru-Guzik, and Marc A. Baldo

The Journal of Chemical Physics COMMUNICATION scitation.org/journal/jcp

Discovery of blue singlet exciton fission molecules via a high-throughput virtual screening and experimental approach

Cite as: J. Chem. Phys. 151, 121102 (2019); doi: 10.1063/1.5114789
Submitted: 11 June 2019 • Accepted: 28 August 2019 •
Published Online: 24 September 2019

Collin F. Perkinson,[1] Daniel P. Tabor,[2,a)] Markus Einzinger,[3] Dennis Sheberla,[2,b)] Hendrik Utzat,[1] Ting-An Lin,[3] Daniel N. Congreve,[4] Moungi G. Bawendi,[1,c)] Alán Aspuru-Guzik,[2,5,c)] and Marc A. Baldo[3,c)]

AFFILIATIONS

[1]Department of Chemistry, Massachusetts Institute of Technology, Cambridge, Massachusetts 02139, USA
[2]Department of Chemistry and Chemical Biology, Harvard University, Cambridge, Massachusetts 02138, USA
[3]Department of Electrical Engineering and Computer Science, Massachusetts Institute of Technology, Cambridge, Massachusetts 02139, USA
[4]Rowland Institute at Harvard University, Cambridge, Massachusetts 02142, USA
[5]Department of Chemistry and Department of Computer Science, University of Toronto, Toronto, Ontario M5S 3H6, Canada

Note: This paper is part of the JCP Special Collection on Singlet Fission.
[a)]**Current address:** Department of Chemistry, Texas A&M University, College Station, Texas 77843, USA.
[b)]**Current address:** Kebotix, Inc., Cambridge, MA 02139, USA.
[c)]**Authors to whom correspondence should be addressed:** mgb@mit.edu; alan@aspuru.com; and baldo@mit.edu

ABSTRACT

Singlet exciton fission is a mechanism that could potentially enable solar cells to surpass the Shockley-Queisser efficiency limit by converting single high-energy photons into two lower-energy triplet excitons with minimal thermalization loss. The ability to make use of singlet exciton fission to enhance solar cell efficiencies has been limited, however, by the sparsity of singlet fission materials with triplet energies above the bandgaps of common semiconductors such as Si and GaAs. Here, we employ a high-throughput virtual screening procedure to discover new organic singlet exciton fission candidate materials with high-energy (>1.4 eV) triplet excitons. After exploring a search space of 4482 molecules and screening them using time-dependent density functional theory, we identify 88 novel singlet exciton fission candidate materials based on anthracene derivatives. Subsequent purification and characterization of several of these candidates yield two new singlet exciton fission materials: 9,10-dicyanoanthracene (DCA) and 9,10-dichlorooctafluoroanthracene (DCOFA), with triplet energies of 1.54 eV and 1.51 eV, respectively. These materials are readily available and low-cost, making them interesting candidates for exothermic singlet exciton fission sensitization of solar cells. However, formation of triplet excitons in DCA and DCOFA is found to occur via hot singlet exciton fission with excitation energies above ~3.64 eV, and prominent excimer formation in the solid state will need to be overcome in order to make DCA and DCOFA viable candidates for use in a practical device.

INTRODUCTION

Introduction to singlet exciton fission

Singlet exciton fission is a down-conversion process in organic semiconductors that spontaneously converts one spin-singlet electron-hole pair (exciton) into two spin-triplet excitons.[1] Each triplet exciton carries approximately half the energy of the initial singlet exciton. Conventional single-junction solar cells are limited in efficiency to about 34% (the Shockley-Queisser limit), largely due to loss from unabsorbed below-bandgap photons and thermalization of high-energy excitons.[2] When combined with a lower-bandgap semiconductor, singlet exciton fission materials raise the theoretical efficiency limit of a single-junction solar cell by reducing thermalization of excitons generated by high-energy

photons. It has been calculated that the maximum power conversion efficiency of a single-junction photovoltaic device incorporating a layer of materials that can undergo singlet exciton fission is 44.4%.[3]

On its own, singlet exciton fission yields no advantage to the power efficiency of solar cells because the potential increase in photocurrent is matched by a decrease in the open circuit voltage.[4] A benefit can be realized, however, if a singlet fission material is matched with a second material that absorbs low-energy photons. For example, in combination with silicon, a singlet exciton fission material ideally absorbs all photons with energies greater than twice the silicon bandgap.[5] The resulting excitons are split into two excitons at or just above the silicon bandgap and transferred to silicon, where they supplement silicon photocurrent generated from direct absorption of photons with energies between the silicon bandgap and twice the silicon bandgap.[6]

Singlet exciton fission requires that the energy of the singlet exciton is approximately twice the energy of the triplet exciton. The exchange energy splitting between singlet and triplet excitons scales with the degree of overlap between the highest occupied molecular orbital and the lowest unoccupied molecular orbital.[7] As a result, most polyacene molecules exhibit singlet-triplet exchange energies of approximately 1.0–1.3 eV.[8] The ideal singlet exciton energy of a singlet fission material is therefore approximately 2.0–2.6 eV; above this singlet energy, fission is typically exothermic, while below this singlet energy, fission is typically endothermic. Indeed, the best-known blue fission material, anthracene, is only capable of hot fission, an inefficient process where the dissociation of singlet excitons competes with internal conversion and vibrational relaxation.[9,10] Modifying anthracene by incorporating chemical side groups can perturb its singlet and triplet energies to make singlet exciton fission thermodynamically feasible directly from the S_1 singlet state. To date, however, such anthracene derivatives have reported triplet energies around 1.1–1.2 eV, providing minimal enthalpic driving force for sensitization of silicon solar cells.[11,12]

The bluest, efficient class of singlet exciton fission materials is based on a core of tetracene, with a singlet exciton energy of approximately 2.4 eV. Fission of these excitons yields triplets with energies almost identical in energy to the silicon bandgap.[1,13] At these energies in the short wavelength infrared, molecules are typically weakly luminescent. Thus, coupling dark triplet excitons to photons for sensitization of photovoltaics requires the use of inorganic materials such as PbS nanocrystals, but with minimal energetic allowance for their Stokes shift or the spectral width of their photoluminescence.[2,14–16]

To improve the prospects of radiative coupling of triplet excitons to silicon, here we employ high-throughput virtual screening (HTVS) to search for blue exciton fission materials based on an anthracene core. We seek to find viable singlet exciton fission candidates with triplet exciton energies in excess of 1.4 eV. The triplet energy threshold of 1.4 eV is chosen because it should allow for exothermic transfer of the triplet excitons to silicon (with a bandgap of about 1.1 eV), even after accounting for uncertainty in calculated triplet energies.

Introduction to high-throughput virtual screening

High-throughput virtual screening (HTVS) combines quantum chemical calculations and cheminformatics methods to reduce a large molecular space to a set of promising leads that experimental chemists can then synthesize and characterize.[17–26] Functional organic molecules are particularly well-suited for high-throughput virtual screening, since the important properties of the materials can be approximated by studying individual molecules in the material, often with relatively computationally inexpensive methods, such as density functional theory (DFT).[18,19]

RESULTS

Library generation

In order to limit our parameter space, we focus on known molecules with an anthracene core and a smaller fraction of combinatorically generated anthracene derivatives, in contrast to the large combinatorial fragment-based libraries that are often employed in high-throughput virtual screening projects for organic materials.[11,27–29] The chemical space of this study consists of known and commercially available molecules. The libraries are obtained by searching eMolecules and Reaxys databases for molecules with an anthracene substructure. A total of 4482 candidates are examined.

Calculation method and benchmark

Before running full-scale calculations, we benchmark several methods to predict S_1 and T_1 values. In order to test the calculations, we use a dataset of 26 published molecules with experimentally determined S_1 and T_1 energies. Since a large contribution from a multireference character in the ground state is not expected, standard hybrid DFT methods are employed. The overall pipeline for calculations is outlined in Fig. 1(a). At the first stage, molecules encoded as Simplified Molecular-Input Line-Entry System (SMILES) strings from the generated library are fed into a conformer generator. The conformer generator samples conformers using a random distance matrix method, as implemented in RDKit.[30] The samples generated are optimized using the MMFF94 force field[31] and duplicates are eliminated. Next, the conformers are optimized using the DFT-B3 method,[32] which gives improved ground state geometries for pi-conjugated systems compared to the MMFF94 force field, and duplicates are again eliminated. The DFT calculations are performed using the OChem 4.0 package.[33] The DFT-B3 conformers are optimized at the B3LYP/6-31G(d) level of theory for both singlet and triplet ground state electron configurations. Finally, excited state calculations are performed on the S_0 geometry of the optimized conformers with three commonly used functionals: hybrid B3LYP,[34] range-separated ωB97X-D,[35] and range-separated ωLC-PBE0,[36,37] using the 6-31G(d) basis set.

For the calibration dataset, B3LYP/6-31G(d) outperforms both of the range-separated functionals with respect to predicting S_1 and T_1 energies (Figs. S1 and S2). We compare two approaches of calculating T_1 energies: vertical time-dependent DFT and a method where triplet energies are estimated by calculating the energy difference between the optimized structures at the ground state and the triplet excited state (calculated using open-shell DFT). The latter performs better in predicting T_1 energies (Fig. S2). With these considerations in mind, we select the pipeline depicted in Fig. 1(a) for calculations of the full candidate material library.

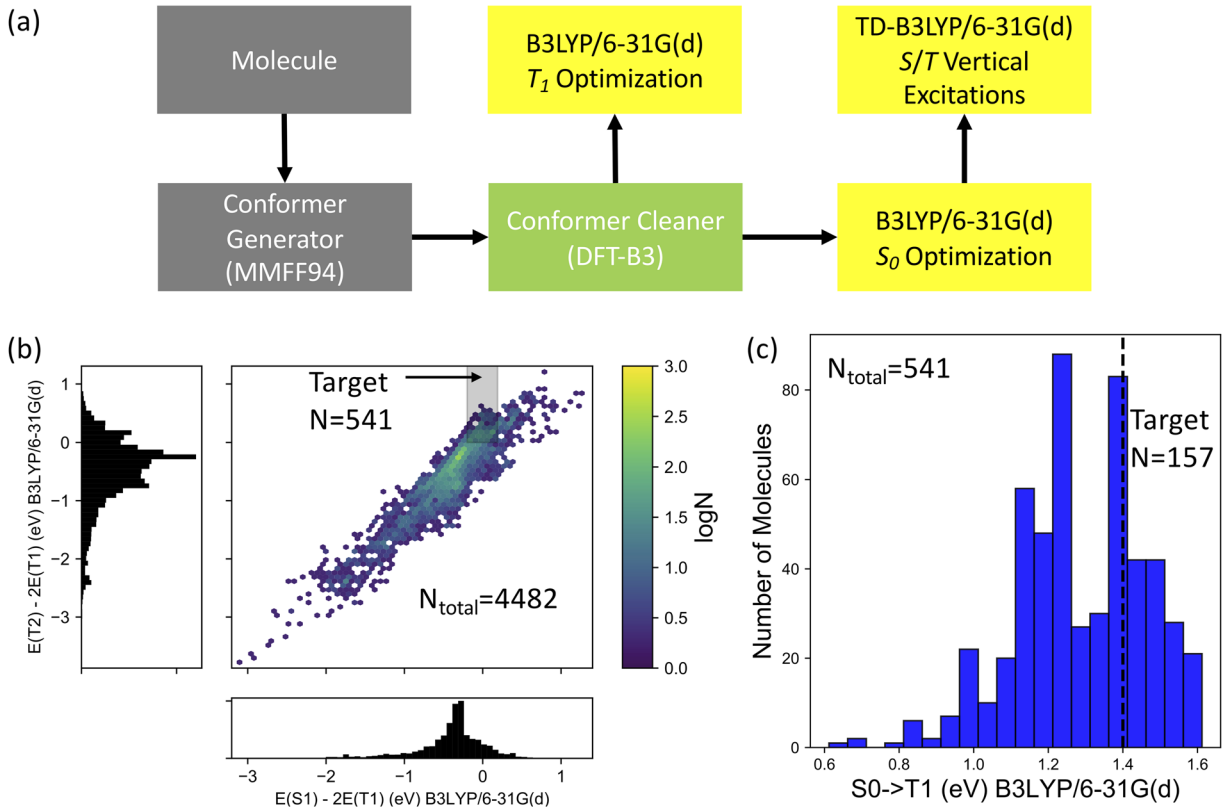

FIG. 1. Calculation pipeline and screening criteria for singlet exciton fission candidates. (a) Computational workflow. (b) Density plot showing the calculated electronic structure of 4482 singlet exciton fission candidate materials resulting from the search from eMolecules. The shaded region indicates the molecules for which $S_1 = 2T_1 \pm 0.2$ eV and $T_2 > 2T_1$, which are the first two criteria applied to screen singlet exciton fission candidates. (c) Distribution of T_1 adiabatic energies for the molecules in the shaded region of (b). The vertical dashed line is at 1.4 eV, an approximate threshold for triplet energy transfer to silicon, when accounting for uncertainty in the molecular candidate excited state calculations.

Computational screening results

In this section, we describe our successive criteria for narrowing the library of 4482 molecules to the most promising blue-absorbing singlet exciton fission candidates for exothermic coupling to silicon solar cells. The first two criteria [depicted in Fig. 1(b)] are related to maximizing the energy level compatibility of the S_1 and T_1 states for singlet exciton fission. In Fig. S3(a), the distributions of calculated S_1 and T_1 energies are jointly plotted. The shaded region indicates the region where the differences between the S_1 energy and twice the T_1 energy are within 0.2 eV of each other, which we use as the cutoff for compatibility, given the observation that singlet exciton fission in tetracene is about 0.2 eV uphill.[38] About 20% of the library satisfies this criterion (929 molecules). The second criterion, which evaluates the difference between the T_2 and T_1 energies, is motivated by the desire to avoid molecules for which two T_1 excitons could upconvert into a T_2 exciton. The shaded region in Fig. 2(b) shows the 541 molecules for which $T_2 > 2T_1$ and for which the S_1/T_1 criterion is satisfied.

Next, we screen for materials with T_1 energies above 1.4 eV, reducing the number of eligible candidates to 157 [Fig. 1(c)]. Of the 384 molecules that are removed at this stage, the vast majority contain tetracene or anthraquinone substructures.

To maximize the probability that the molecules will perform well in an aggregate structure, we seek to minimize the variance in the conformer excited state energies. Screening for molecules where the range of S_1 and T_1 adiabatic excitation energies is less than 0.05 eV further reduces the number of eligible candidate materials to 116 (Figs. S4 and S5). As expected from chemical principles, most of the molecules excluded at this stage contain multiple rotatable bonds, often to another aromatic ring.

We next screen for molecules with S_1 energies predominantly in the blue but not in the UV, since such molecules are better suited to the solar spectrum and may be less susceptible to photoinduced chemical degradation. This corresponds to an $S_0 \rightarrow S_1$ transition between 2.64 eV and 3.26 eV. Of the 116 molecules remaining before this criterion, all absorb in this range (Fig. S6). However, this criterion would exclude some molecules if a lower T_1 cutoff energy (such as 1.2 eV) is employed for compatibility to Si, and it could also be a useful screening criterion for larger libraries.

Finally, to narrow the focus of our study to true anthracene derivatives, we filter out the remaining molecules containing more

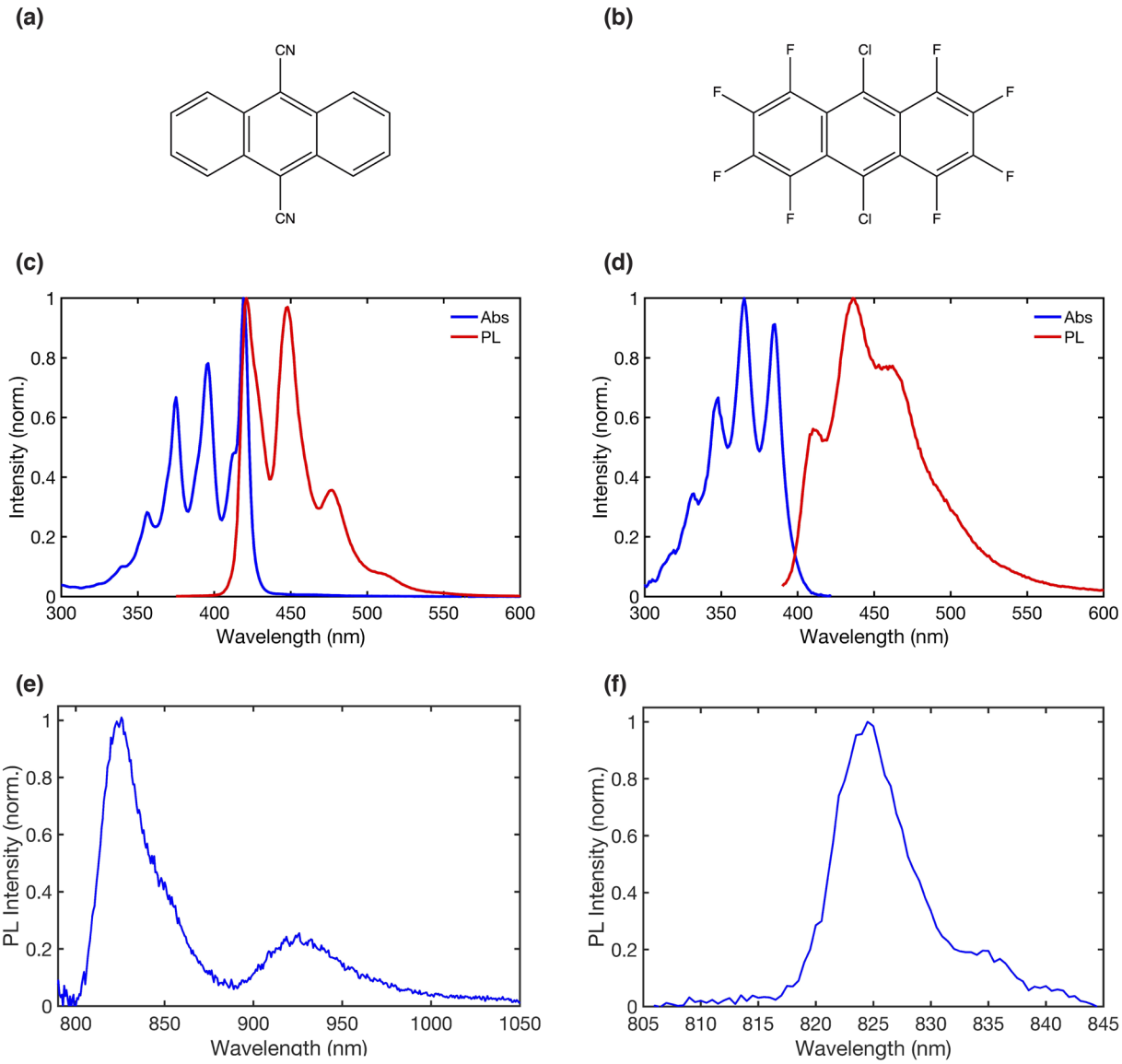

FIG. 2. Steady-state optical characterization of DCA and DCOFA. Chemical structures of (a) DCA and (b) DCOFA. Absorbance and fluorescence of dilute solutions of (c) DCA in cyclohexane and (d) DCOFA in chloroform. (e) Triplet phosphorescence of a drop-cast film of DCA doped at 2 wt. % in 4BrPS, obtained at 77 K, using out-of-phase optical choppers to filter out prompt singlet emission. (f) Triplet phosphorescence of a drop-cast film of DCOFA doped at 2 wt. % in $[PMMA:BP]_{3:1}$ at room temperature. Delayed singlet emission resulting from triplet-triplet annihilation is subtracted from the original spectra to obtain these results, as detailed in Fig. S7. The rising edges of the phosphorescence indicate triplet energies of 1.54 eV and 1.51 eV for DCA and DCOFA, respectively.

than five fused rings, leaving us with 88 singlet exciton fission candidate materials, approximately 2.0% of our original library.

Experimental characterization of singlet exciton fission candidates

From the pool of 88 singlet exciton fission candidate materials, two are chosen for experimental characterization: 9,10-dicyanoanthracene (DCA) and 9,10-dichlorooctafluoroanthracene (DCOFA). DCA and DCOFA are selected for this study because their calculated triplet energies are high (1.47 eV and 1.45 eV, respectively), making them promising candidates for exothermic triplet transfer and sensitization of silicon. Additionally, both DCA and DCOFA have known crystal structures reported in the Cambridge Crystallographic Data Centre and are readily available from commercial suppliers, having been used as synthetic precursors in prior experimental studies.[39–41] Furthermore, both materials are reported to have a single conformer, and therefore, issues related

to stacking and energy mismatch between conformers should be minimized. DCA and DCOFA are purchased from Sigma-Aldrich and further purified using a sublimation furnace. Their chemical structures are shown in Figs. 2(a) and 2(b).

To confirm the calculated singlet energies of DCA and DCOFA, steady-state absorbance and photoluminescence spectra are measured [Figs. 2(c) and 2(d)]. Both materials exhibit absorbance spectra with a clear vibrational structure. From the onset of their bluest emission features, we estimate the S_1 energies of DCA and DCOFA in solution to be 2.99 eV and 3.10 eV, respectively, compared to the calculated values of 2.98 eV and 2.97 eV. Note that these singlet energies are likely to vary slightly depending on the specific solvent chosen.[42]

To prepare for measuring the triplet energy of DCA, the material is dropcast from solution at 2 wt. % in poly(4-bromostyrene) (4BrPS), at a total concentration of ~20 mg/ml in methoxybenzene. At 2 wt. %, it is not expected that DCA undergoes efficient singlet exciton fission. That said, the presence of bromine in the host material causes enhanced intersystem singlet-to-triplet crossing via spin-orbit coupling and the heavy-atom effect.[43] Moreover, as methoxybenzene dries, 4BrPS forms a rigid polymer matrix, which is expected to reduce nonradiative recombination from coupling to molecular vibronic modes.[44] The film is encapsulated in a nitrogen glovebox before being transferred to a cryostat and pumped down to ~1×10^{-7} Torr at a temperature of 77 K.

To experimentally measure T_1 phosphorescence from DCA, we employ an optical gating method using out-of-phase choppers to mechanically filter out prompt emission and capture only delayed emission, which is expected to result from longer-lived triplet state emission [as well as delayed emission following subsequent triplet-triplet (TT) fusion back to the singlet state]. The resulting spectrum (after subtraction of singlet emission, Fig. S7) is shown in Fig. 2(e).

To measure DCOFA phosphorescence, we use a room temperature phosphorescence method described by Reineke and Baldo.[44] DCOFA is doped in a film of PMMA and benzophenone (BP), a well-known triplet sensitizer with an intersystem crossing efficiency close to 100% at room temperature[45] and a triplet energy of 2.96 eV.[44] The film is excited at 270 nm, where BP absorbs strongly, and the resulting emission spectrum is compared to the spectrum when excited at 385 nm, where DCOFA is the dominant absorber. Subtracting the neat DCOFA singlet exciton spectrum from the spectrum of DCOFA doped in BP yields the phosphorescence spectrum shown in Fig. 2(f).

The triplet energies of DCA and DCOFA are estimated from the onset of their emission to be 1.54 eV and 1.51 eV, respectively (compared to the calculated triplet energies of 1.47 eV and 1.45 eV). The experimental triplet energies of DCA and DCOFA are in close agreement with the values calculated during material screening, as summarized in Table I.

To demonstrate that DCA and DCOFA undergo singlet exciton fission, we measure the magnetic field effect (MFE) on photoluminescence intensity. The theory of MFEs in organic molecular crystals was developed by Merrifield in 1968.[46] When a molecule undergoes singlet exciton fission, it forms a triplet-triplet pair state with an overall spin-singlet character. Singlet excitons can only effectively couple to the subpopulation of the nine possible triplet-triplet (TT) pair states with a singlet character. In the absence of a magnetic field, only three of the nine TT states have partial singlet character. As the field increases, the small splitting in triplet energies results in more of the TT states developing the singlet character, thus increasing the rate of singlet exciton fission (and resulting in an initially negative MFE on the singlet PL intensity). As the magnetic field is increased further, the number of TT states with singlet character decreases to two, consequently reducing the rate of singlet exciton fission (and resulting in a positive MFE on the singlet PL intensity at higher magnetic fields). The typical MFE signature of singlet exciton fission is therefore a negative MFE at low fields, switching to a positive MFE at higher fields, which plateaus as the magnetic field is increased and the number of TT states with singlet character approaches two.

TABLE I. Comparison of singlet and triplet energies from experiment and theory. Singlet and triplet energies calculated with density functional theory (DFT), compared against experimentally measured values.

DCA	Theory (eV)	Experiment (eV)
S_1	2.98	2.99
T_1	1.47	1.54
DCOFA	**Theory (eV)**	**Experiment (eV)**
S_1	2.97	3.10
T_1	1.45	1.51

Figure 3 shows the MFE on singlet photoluminescence from purified DCA and DCOFA crystals under 340 nm light-emitting diode (LED) excitation. Both DCA and DCOFA exhibit a nonmonotomic, positive MFE with zero-MFE crossings at ~0.1 T, characteristic of singlet exciton fission. Curiously, however, the MFE on photoluminescence in DCA and DCOFA is inverted when using excitation wavelengths longer than 340 nm and 365 nm, respectively (Fig. S8). To make sense of these differences, we suggest that the observed MFE shapes reflect changes in the origin of delayed fluorescence for varying pump wavelengths. A positive MFE, as is observed under 340 nm excitation, suggests that delayed fluorescence is due to the annihilation of correlated triplet excitons originally formed by singlet exciton fission, as described above. Meanwhile, the inverted and negative MFE observed at longer excitation wavelengths is indicative of delayed fluorescence due to the annihilation of initially uncorrelated triplet excitons (possibly formed through weak intersystem crossing). We speculate therefore that, as in neat anthracene,[9,10] singlet exciton fission in DCA and DCOFA is mediated by excited states above S_1, while at longer excitation wavelengths, singlet exciton fission is unfavorable.

Indeed, the highest-energy emission peaks from DCA and DCOFA are red-shifted by around 100 nm in crystalline powder as compared to those in solution (Fig. S9). Based on this red-shift and their large spectral width, the prompt emission peaks in Fig. S9 likely contain contributions from emissive excimer states of DCA and DCOFA. From the rising edge of the crystalline DCA and DCOFA prompt emission peaks, we estimate the energies of these states to be 2.59 eV and 2.71 eV, respectively, making singlet exciton fission uphill by more than 300 meV in each case. The substantial endothermicity associated with splitting such states into two triplets further suggests that singlet exciton fission in crystalline DCA and DCOFA is mediated by excited states above S_1.

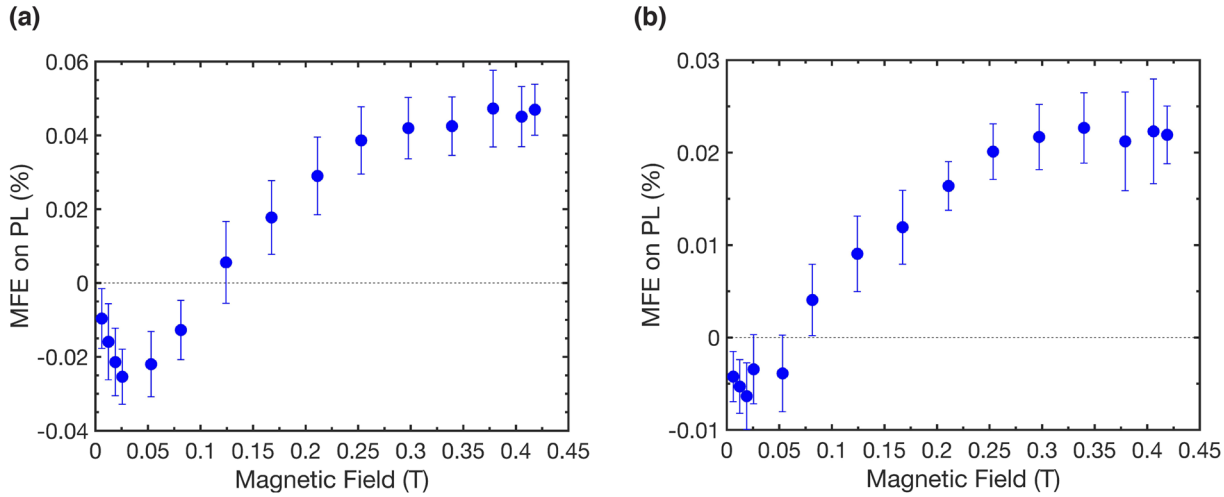

FIG. 3. Evidence of singlet exciton fission. Relative change in fluorescence at 340 nm excitation from purified crystals of (a) DCA and (b) DCOFA as a function of external magnetic field. The change in fluorescence is positive for both samples at higher field strengths, with a zero-MFE crossing at 0.05–0.1 T, strongly suggesting that both materials undergo singlet exciton fission.

Hot singlet exciton fission has previously been reported in anthracene, tetracene, and several other organic crystalline semiconductors.[8,9,47] Hot fission in these materials has generally been attributed to coupling of the TT pair state to vibrationally excited states,[48,49] with recent studies emphasizing the importance of excited states with charge-transfer (CT) character.[50,51] Given the excitation wavelength dependence that we observe in the MFE of DCA and DCOFA, it is possible that singlet exciton fission in these materials is mediated by an excited CT state. Rational design of DCA and DCOFA dimers could be used to reduce excimer formation and make singlet exciton fission from the ground excited state more favorable.[52]

CONCLUSION

In this study, we employ high-throughput virtual screening to reduce an initial set of 4482 singlet exciton fission candidate materials to a list of 88 candidates with calculated triplet energies in excess of 1.4 eV. The effectiveness of the virtual screening procedure is demonstrated via the discovery of two new singlet exciton fission materials: DCA and DCOFA. These materials are readily available, low-cost, and have high triplet energies (~1.5 eV), making them promising candidates for exothermic singlet exciton fission sensitization of solar cells. Practical use of DCA and DCOFA as singlet fission materials is limited, however, by substantial excimer formation in the solid-state, requiring excitation wavelengths of ~340 nm or lower in order to observe singlet exciton fission. Further tailoring of molecular coupling in DCA and DCOFA, for example through dimerization, may reduce excimer formation and make these materials more practical for use in a device. Integrating intermolecular coupling into virtual screening criteria is expected to result in higher hit rates for screened materials. This study shows that computational screening can lead to molecules that have necessary but not sufficient properties for function, highlighting one of the most important challenges and opportunities in the field of virtual high-throughput virtual screening.

EXPERIMENTAL METHODS

Materials

The materials used have acronyms as follows. DCA: 9,10-dicyanoanthracene, DCOFA: 9,10-dichlorooctafluoroanthracene, 4BrPS: poly(4-bromostyrene), MB: methoxybenzene, BP: benzophenone, and PMMA: poly(methyl 2-methylpropenoate). All materials except DCA and DCOFA were used as received without further purification. DCA (>99.7% sublimed grade) and DCOFA (>99% sublimed grade) were further purified via sublimation in a tube furnace. The experimental work in this manuscript relied on the material deposited near the center of the tube furnace, since this region had the lowest temperature gradient and was expected to yield the purest material. Further details on material purification are included in the supplementary material. Vendor information: DCA, DCOFA, 4BrPS, MB, chloroform, and cyclohexane: Sigma Aldrich; PMMA: Alfa Aesar.

Steady-state absorbance

Absorbance spectra in solution were collected using a UV-Vis absorbance spectrometer (Cary 5000, Agilent). Samples were prepared by dissolving purified DCA and DCOFA in cyclohexane and chloroform, respectively. All solution absorbance measurements were made using 1 cm path length quartz cuvettes.

Solid-state absorbance spectra of purified, crystalline powders of DCA and DCOFA were obtained by diffuse reflection (Cary 5000, Agilent). KBr was used as a reference, and the powders were diluted at 1 wt. % in KBr. The measured reflectance was converted to the Kubelka-Munk parameter, which is proportional to the absorption coefficient.

Singlet state photoluminescence

Photoluminescence spectra were collected using a spectrofluorometer (Fluoromax-3, Horiba). To minimize spectral distortion due to reabsorption, samples were diluted so that the optical density at their peak absorbance wavelengths is below 0.03 cm^{-1}. All spectra were collected using an excitation wavelength of 375 nm with entrance and exit slits set at a bandpass of 5 nm and 1 nm, respectively.

Triplet state phosphorescence

DCA phosphorescence was measured using a thermoelectrically cooled silicon camera (PRO-EM-HS:512BX3, Princeton Instruments). Samples were prepared using 5 mm × 5 mm quartz substrates (MTI Corp). The substrates were cleaned via sequential sonication in detergent solution (Micro-90), deionized water, and acetone. They were then immersed in boiling isopropanol, dried with a nitrogen spray gun, and transferred to a nitrogen glovebox. Solutions of 4BrPS (20 mg/ml in MB) and DCA (1 mg/ml in MB) were prepared and subsequently combined to form a solution of DCA (2 wt. % in 4BrPS). Films of DCA/4BrPS were formed via dropcasting onto the quartz substrates at 70 °C and maintaining at 70 °C until dry. Samples were encapsulated in the glovebox using a UV curable epoxy (OG159-2, Epoxy Technology) and a second, 2-side polished quartz substrate (MTI Corp).

Samples were then loaded into a helium closed-cycle cryostat (Montana), pumped under vacuum to 1 × 10^{-7} Torr, and cooled to 77 K. Phosphorescence spectra were obtained using two chopper wheels operated out-of-phase using phase-locked chopper controllers (MC2000B, Thorlabs) to time-gate sample excitation and emission collection, so as to block prompt emission and collect only the delayed portion of the photoluminescence. A 340 nm LED (M340L4, Thorlabs) was used for excitation, chopped at 270 Hz, defining approximately 2 ms optical gates. Sample emission was collimated, refocused into a monochromator (SP-2300, Princeton Instruments), and subsequently imaged on a thermoelectrically cooled silicon camera (PRO-EM-HS:512BX3, Princeton Instruments). Both singlet photoluminescence and triplet phosphorescence contributed to the recorded spectra. To remove the contribution from singlet emission, the blue portion of the emission spectrum (from 450 to 700 nm) was fit to the 77 K ungated singlet emission spectrum, and the singlet PL contribution was subtracted from the measured spectrum, yielding the phosphorescence spectrum shown in Fig. 2(c).

DCOFA phosphorescence was measured at room temperature according to a method adapted from Reineke *et al.*[44] A 20 mg/ml solution of DCOFA doped at 2 wt. % in $[PMMA:BP]_{3:1}$ was prepared and dropcast from methoxybenzene onto a cleaned 10 mm × 10 mm quartz substrate at 70 °C in a nitrogen glovebox. Once dry, the sample was encapsulated using a second quartz substrate and a UV curable epoxy. Phosphorescence was detected on a spectrofluorometer (Fluoromax-3, Horiba) by exciting the sample at 270 nm (where BP absorbs) and comparing against spectra obtained at 385 nm excitation (where only DCOFA absorbs). To remove the contribution from singlet emission, the blue portion of the emission spectra (from 450 to 700 nm) was fit and the singlet PL contribution was subtracted from the measured spectrum, yielding the phosphorescence spectrum shown in Fig. 2(d).

Magnetic field effect

Measurements of the magnetic field effect on DCA and DCOFA photoluminescence were performed according to the procedure described by Congreve *et al.*[4] A monochromatic 340 nm light-emitting diode (M340L4, Thorlabs) was used to excite the samples. Light from the diode was cleaned with a bandpass filter and mechanically chopped. While the sample was under illumination, an electromagnet was switched between positive and zero magnetic fields at a frequency of 33 mHz and a duty cycle of 50%. A 400 nm longpass filter was used to filter the scatter from the LED and ensure that only sample emission was detected, while a 750 nm shortpass filter was used to ensure that any phosphorescence that might contribute to the sample emission at room temperature was excluded. Photoluminescence from the sample was detected using a silicon photodetector (818-UV, Newport) connected to a lock-in amplifier (SR830, Stanford Research Systems). The magnetic field was monitored using a transverse gaussmeter probe (HMMT-6J04-VF, Lakeshore). The emission intensity and magnetic field were recorded at a frequency of 1 Hz.

For each data point in the plot of the magnetic field effect, the change in photoluminescence was calculated using the following steps: First, the photoluminescence was averaged over the full period in which the positive magnetic field was applied. Second, the PL was averaged over the full period in which the magnetic field was zero. The amplitude of the magnetic field effect is then given by the relative change in signal percentage, $MFE = 100\% * (PL_B - PL_0)/PL_0$, where PL_B and PL_0 are the averaged emission intensities with and without applied magnetic field.

Powder x-ray diffraction

Powder x-ray diffraction PXRD patterns were measured on purified, crystalline powders of DCA and DCOFA using a diffractometer (Advance II, Bruker) equipped with θ/2θ Bragg-Brentano geometry and Ni-filtered Cu Kα radiation ($K\alpha_1$ = 1.5406 Å, $K\alpha_2$ = 1.5444 Å, $K\alpha_1/K\alpha_2$ = 0.5). The tube voltage and current were set to 40 kV and 40 mA, respectively. Samples were prepared as a thin layer of powder on a zero-background silicon crystal plate. The angle was scanned from 2θ = 3°–50° in increments of 0.02° using a slit size of 1.0 mm and a scan rate of 1 s/step and resulting PXRD patterns compared to calculated patterns from the data reported in the Cambridge Crystallographic Data Centre.

SUPPLEMENTARY MATERIAL

See the supplementary material for additional figures related to the materials screening procedure and experimental characterization. A full list of singlet exciton fission calibration data and candidate materials considered for this study is included in the associated spreadsheet files uploaded with this manuscript.

ACKNOWLEDGMENTS

C.F.P. was supported by the Center for Excitonics, an Energy Frontier Research Center funded by the U.S. Department of Energy, Office of Science, Office of Basic Energy Sciences, under Award No. DE-SC0001088 (MIT). C.F.P. was also supported by the National Science Foundation Graduate Research Fellowship under Grant No.

1122374. M.E. and T.-A.L. were supported by the U.S. Department of Energy, Office of Basic Energy Sciences (Award No. DE-FG02-07ER46474). H.U. was funded by the U.S. Department of Energy, Office of Basic Energy Sciences, Division of Materials Sciences and Engineering (Award No. DE-FG02-07ER46454). D.N.C. acknowledges the support of the Rowland Fellowship at the Rowland Institute at Harvard University. D.P.T. and A.A.-G were funded by the Innovation Fund Denmark via the Grand Solutions project "ORBATS" (File No. 7045-00018B). D.S. and A.A.-G. were supported by the Harvard Climate Solution Fund. A.A.-G. was additionally supported by the Canada 150 Research Chair Program, as well as generous support from Anders Frøseth. The authors would also like to thank Dong-Gwang Ha and Ruomeng Wan for their assistance in collecting the PXRD and solid-state absorbance measurements reported in Figs. S9–S11.

The authors declare no competing financial interests.

REFERENCES

[1] M. B. Smith and J. Michl, "Singlet fission," Chem. Rev. **110**, 6891–6936 (2010).
[2] A. Rao and R. H. Friend, "Harnessing singlet exciton fission to break the Schokley-Queisser limit," Nat. Rev. Mater. **2**, 17063 (2017).
[3] M. C. Hanna and A. J. Nozik, "Solar conversion efficiency of photovoltaic and photoelectrolysis cells with carrier multiplication absorbers," J. Appl. Phys. **100**, 074510 (2006).
[4] D. N. Congreve, J. Lee, N. J. Thompson, E. Hontz, S. R. Yost, P. D. Reusswig, M. E. Bahlke, S. Reineke, T. Van Voorhis, and M. A. Baldo, "External quantum efficiency above 100% in a singlet-exciton-fission–based organic photovoltaic cell," Science **340**, 334–337 (2013).
[5] D. L. Dexter, "Two ideas on energy transfer phenomena: Ion-pair effects involving the OH stretching mode, and sensitization of photovoltaic cells," J. Lumin. **18**, 779–784 (1979).
[6] M. Einzinger, T. Wu, J. F. Kompalla, H. L. Smith, C. F. Perkinson, L. Nienhaus, S. Wiefhold, D. N. Congreve, A. Kahn, M. G. Bawendi, and M. A. Baldo, "Sensitization of silicon by singlet exciton fission in tetracene," Nature **571**, 90–94 (2019).
[7] S. Vosskötter, P. Konieczny, C. Marian, and R. Weinkauf, "Towards an understanding of the singlet-triplet splittings in conjugated hydrocarbons: Azulene invensitaged by anion photoelectron spectroscopy and theoretical calculations," Phys. Chem. Chem. Phys. **17**, 23573–23581 (2015).
[8] J. B. Birks, *Photophysics of Aromatic Molecules* (Wiley, London, 1970).
[9] G. Klein and R. Voltz, "Magnetic field effect on prompt fluorescence in anthracene: Evidence for singlet exciton fission," Chem. Phys. Lett. **16**(2), 340–344 (1972).
[10] G. Klein and R. Voltz, "On singlet exciton fission in anthracene and tetracene at 77°K," Chem. Phys. Lett. **19**(3), 391–394 (1973).
[11] B. Manna, A. Nandi, and R. Ghosh, "Ultrafast singlet exciton fission dynamics in 9,10-bis(phenylethynyl)anthracene nanoaggregates and thin films," J. Phys. Chem. C **122**, 21047–21055 (2018).
[12] Y. J. Bae, G. Kang, C. D. Malliakas, J. N. Nelson, J. Zhou, R. M. Young, Y.-L. Wu, R. P. Van Duyne, G. C. Schatz, and M. R. Wasielewski, "Singlet exciton fission in 9,10-bis(phenylethynyl)anthracene thin films," J. Am. Chem. Soc. **140**, 15140–15144 (2018).
[13] N. Geacintov, M. Pope, and F. Vogel, "Effect of magnetic field on the fluorescence of tetracene crystals: Exciton fission," Phys. Rev. Lett. **22**, 593–596 (1969).
[14] N. J. Thompson, M. W. B. Wilson, D. N. Congreve, P. R. Brown, J. M. Scherer, T. S. Bischof, M. Wu, N. Geva, M. Welborn, T. Van Voorhis, V. Bulovic, M. G. Bawendi, and M. A. Baldo, "Energy harvesting of non-emissive triplet excitons in tetracene by emissive PbS nanocrystals," Nat. Mater. **13**, 1039–1043 (2014).
[15] M. Tabachnyk, B. Ehrler, S. Gélinas, M. L. Böhm, B. J. Walker, K. P. Musselman, N. C. Greenham, R. H. Friend, and A. Rao, "Resonant energy transfer of triplet excitons from pentacene to PbSe nanocrystals," Nat. Mater. **13**, 1033–1038 (2014).
[16] M. H. Futscher, A. Rao, and B. Ehrler, "The potential of singlet fission photon multipliers as an alternative to silicon-based tandem solar cells," ACS Energy Lett. **3**, 2587–2592 (2018).
[17] E. O. Pyzer-Knapp, C. Suh, R. Gómez-Bombarelli, J. Aguilera-Iparraguirre, and A. Aspuru-Guzik, "What is high-through virtual screening? A perspective from organic materials discovery," Annu. Rev. Mater. Res. **45**, 195–216 (2015).
[18] R. Gómez-Bombarelli, J. Aguilera-Iparraguirre, T. D. Hirzel, D. Duvenaud, D. Maclaurin, M. A. Blood-Forsyth, H. S. Chae, M. Einzinger, D.-G. Ha, T. Wu, G. Markopoulos, S. Jeon, H. Kang, H. Miyazaki, M. Numata, S. Kim, W. Huang, S. I. Hong, M. Baldo, R. P. Adams, and A. Aspuru-Guzik, "Design of efficient molecular organic light-emitting diodes by a high-throughput virtual screening and experimental approach," Nat. Mater. **15**, 1120–1127 (2016).
[19] K. J. Fallon, P. Budden, E. Salvadori, A. M. Ganose, C. N. Savory, L. Eyre, S. Dowland, Q. Ai, S. Goodlett, C. Risko, D. O. Scanlon, C. W. M. Kay, A. Rao, R. H. Friend, A. J. Musser, and H. Bronstein, "Exploiting excited-state aromaticity to design highly stable singlet fission materials," J. Am. Chem. Soc. **141**(35), 13867–13876 (2019).
[20] K. Alberi, M. B. Nardelli, A. Zakutayev, L. Mitas, S. Curtarolo, A. Jain, M. Fornari, N. Marzari, I. Takeuchi, M. L. Green, M. Kanatzidis, M. F. Toney, S. Butenko, B. Meredig, S. Lany, U. Kattner, A. Davydov, E. S. Toberer, V. Stevanovic, A. Walsh, N.-G. Park, A. Aspuru-Guzik, D. P. Tabor, J. Nelson, J. Murphy, A. Setlur, J. Gregoire, H. Li, R. Xiao, A. Ludwig, L. W. Martin, A. M. Rappe, S.-H. Wei, and J. Perkins, "The 2019 materials by design roadmap," J. Phys. D: Appl. Phys. **52**, 013001 (2018).
[21] A. Jain, Y. Shin, and K. A. Persson, "Computational predictions of energy materials using density functional theory," Nat. Rev. Mater. **1**, 15004 (2016).
[22] J. Hachmann, R. Olivares-Amaya, A. Jinich, A. L. Appleton, M. A. Blood-Forsythe, L. R. Seress, C. Román-Salgado, K. Trepte, S. Atahan-Evrenk, S. Er, S. Shrestha, R. Mondal, A. Sokolov, Z. Bao, and A. Aspuru-Guzik, "Lead candidates for high-performance organic photovoltaics from high-throughput quantum chemistry," Energy Environ. Sci. **7**, 698–704 (2014).
[23] D. P. Tabor, L. M. Roch, S. K. Saikin, C. Kreisbeck, D. Sheberla, J. H. Montoya, S. Dwaraknath, M. Aykol, C. Ortiz, H. Tribukait, C. Amador-Bedolla, C. J. Brabec, B. Maruyama, K. A. Persoon, and A. Aspuru-Guzik, "Accelerating the discovery of materials for clean energy in the era of smart automation," Nat. Rev. Mater. **3**, 5–20 (2018).
[24] L. Cheng, R. S. Assary, X. Qu, A. Jain, S. P. Ong, N. N. Rajput, K. Persson, and L. A. Curtiss, "Accelerating electrolyte discovery for energy storage with high-throughput screening," J. Phys. Chem. Lett. **6**, 283–291 (2015).
[25] I. Y. Kanal, S. G. Owens, J. S. Bechtel, and G. R. Hutchison, "Efficient computational screening of organic polymer photovoltaics," J. Phys. Chem. Lett. **4**, 1613–1623 (2013).
[26] E. Kim, K. Huang, S. Jegelka, and E. Olivetti, "Virtual screening of inorganic materials synthesis parameters with deep learning," npj Comput. Mater. **3**, 53 (2017).
[27] J. Hachmann, R. Olivares-Amaya, S. Atahan-Evrenk, C. Amador-Bedolla, R. S. Sánchez-Carrera, A. Gold-Parker, L. Vogt, A. M. Brockway, and A. Aspuru-Guzik, "The Harvard clean energy project: Large-scale computational screening and design of organic photovoltaics on the world community grid," J. Phys. Chem. Lett. **2**, 2241–2251 (2011).
[28] S. A. Lopez, B. Sanchez-Lengeling, J. de Goes Soares, and A. Aspuru-Guzik, "Design principles and top non-fullerene acceptor candidates for organic photovoltaics," Joule **1**, 857–870 (2017).
[29] N. M. O'Boyle, C. M. Campbell, and G. R. Hutchison, "Computational design and selection of optimal organic photovoltaic materials," J. Phys. Chem. C **115**, 16200–16210 (2011).
[30] G. Landrum, "RDKit: Open-source cheminformatics," https://www.rdkit.org/ (2006).
[31] T. A. Halgren, "MMFF94s option for energy minimization studies," J. Comput. Chem. **20**, 720–729 (1999).
[32] M. Gaus, Q. Cui, and M. Elstner, "DFTB3: Extension of the self-consistent-charge density-functional tight-binding method (SCC-DFTB)," J. Chem. Theory Comput. **7**, 931–948 (2011).

[33]Y. Shao, Z. Gan, E. Epifanovsky, A. T. B. Gilbert, M. Wormit, J. Kussmann, A. W. Lange, A. Behn, J. Deng, X. Feng, D. Ghosh, M. Goldey, P. R. Horn, L. D. Jacobson, I. Kaliman, R. Z. Khaliullin, T. Kús, A. Landau, J. Liu, E. I. Proynov, Y. M. Rhee, R. M. Richard, M. A. Rohrdanz, R. P. Steele, E. J. Sundstrom, H. L. Woodcock III, P. M. Zimmerman, D. Zuev, B. Albrecht, E. Alguire, B. Austin, G. J. O. Beran, Y. A. Bernard, E. Berquist, K. Brandhorst, K. B. Bravaya, S. T. Brown, D. Casanova, C.-M. Chang, Y. Chen, S. H. Chien, K. D. Closser, D. L. Crittenden, M. Diedenhofen, R. A. DiStasio, Jr., H. Dop, A. D. Dutoi, R. G. Edgar, S. Fatehi, L. Fusti-Molnar, A. Ghysels, A. Golubeva-Zadorozhnaya, J. Gomes, M. W. D. Hanson-Heine, P. H. P. Harbach, A. W. Hauser, E. G. Hohenstein, Z. C. Holden, T.-C. Jagau, H. Ji, B. Kaduk, K. Khistyaev, J. Kim, J. Kim, R. A. King, P. Klunzinger, D. Kosenkov, T. Kowalczyk, C. M. Krauter, K. U. Lao, A. Laurent, K. V. Lawler, S. V. Levchenko, C. Y. Lin, F. Liu, E. Livshits, R. C. Lochan, A. Luenser, P. Manohar, S. F. Manzer, S.-P. Mao, N. Mardirossian, A. V. Marenich, S. A. Maurer, N. J. Mayhall, C. M. Oana, R. Olivares-Amaya, D. P. O'Neill, J. A. Parkhill, T. M. Perrine, R. Peverati, P. A. Pieniazek, A. Prociuk, D. R. Rehn, E. Rosta, N. J. Russ, N. Sergueev, S. M. Sharada, S. Sharmaa, D. W. Small, A. Sodt, T. Stein, D. Stück, Y.-C. Su, A. J. W. Thom, T. Tsuchimochi, L. Vogt, O. Vydrov, T. Wang, M. A. Watson, J. Wenzel, A. White, C. F. Williams, V. Vanovschi, S. Yeganeh, S. R. Yost, Z.-Q. You, I. Y. Zhang, X. Zhang, Y. Zhou, B. R. Brooks, G. K. L. Chan, D. M. Chipman, C. J. Cramer, W. A. Goddard III, M. S. Gordon, W. J. Hehre, A. Klamt, H. F. Schaefer III, M. W. Schmidt, C. D. Sherrill, D. G. Truhlar, A. Warshel, X. Xua, A. Aspuru-Guzik, R. Baer, A. T. Bell, N. A. Besley, J.-D. Chai, A. Dreuw, B. D. Dunietz, T. R. Furlani, S. R. Gwaltney, C.-P. Hsu, Y. Jung, J. Kong, D. S. Lambrecht, W. Liang, C. Ochsenfeld, V. A. Rassolov, L. V. Slipchenko, J. E. Subotnik, T. Van Voorhis, J. M. Herbert, A. I. Krylov, P. M. W. Gill, and M. Head-Gordon, "Advances in molecular quantum chemistry contained in the Q-Chem 4 program package," Mol. Phys. **113**, 184–215 (2015).

[34]A. D. Becke, "Density-functional thermochemistry. III. The role of exact exchange," J. Chem. Phys. **98**, 5648–5652 (1993).

[35]J.-D. Chai and M. Head-Gordon, "Long-range corrected hybrid density functionals with damped atom-atom dispersion corrections," Phys. Chem. Chem. Phys. **10**, 6615–6620 (2008).

[36]C. Adamo, G. E. Scuseria, and V. Barone, J. Chem. Phys. **111**, 2889–2899 (1999).

[37]M. A. Rohrdanz and J. M. Herbert, "Simultaneous benchmarking of ground- and excited-state properties with long-range-corrected density functional theory," J. Chem. Phys. **129**, 034107 (2008).

[38]J. J. Burdett, D. Gosztola, and C. J. Bardeen, "The dependence of singlet exciton relaxation on excitation density and temperature in polycrystalline tetracene thin films: Kinetic evidence for a dark intermediate state and implications for singlet fission," J. Chem. Phys. **135**, 214508 (2011).

[39]E. Baciocchi, C. Crescenzi, and C. Lanzalunga, "Photoinduced electron transfer reactions on benzyl phenyl sulfides promoted by 9,10-dicyanoanthracene," Tetrahedron **53**, 4469–4478 (1997).

[40]I. N. Lykakis, S. Lestakis, and M. Orfanopoulos, "9,10-dicyanoanthracene photosensitized oxidation of aryl alkanols: Evidence for an electron transfer mechanism," Tetrahedron Lett **44**, 6247–5251 (2003).

[41]J. F. Tannaci, M. Noji, J. McBee, and T. D. Tilley, "9,10-dichlorooctafluoroanthracene as a building block for n-type organic semiconductors," J. Org. Chem. **72**, 5567–5573 (2007).

[42]A. Olea, D. R. Worrall, F. Wilkinson, S. L. Williams, and A. Abdel-Shafi, "Solvent effects on the photophysical properties of 9,10-dicyanoanthracene," Phys. Chem. Chem. Phys. **4**, 161–167 (2002).

[43]M. Einzinger, T. Zhu, P. de Silva, C. Belger, T. M. Swager, T. Van Voorhis, and M. A. Baldo, "Shorter exciton lifetimes via an external heavy-atom effect: Alleviating the effects of bimolecular processes in organic light-emitting diodes," Adv. Mater. **29**, 1701987 (2017).

[44]S. Reineke and M. A. Baldo, "Room temperature triplet state spectroscopy of organic semiconductors," Sci. Rep. **4**, 3797 (2014).

[45]N. J. Turro, V. Ramamurthy, and J. C. Scaiano, *Modern Molecular Photochemistry of Organic Molecules* (University Science Books, 2010).

[46]R. E. Merrifield, "Theory of magnetic field effects on the mutual annihilation of triplet excitons," J. Chem. Phys. **48**, 4318 (1968).

[47]W. G. Albrecht, H. Coufal, R. Haberkorn, and M. E. Michel-Beyerle, "Excitation spectra of exciton fission in organic crystals," Phys. Stat. Sol. **89**, 261–265 (1978).

[48]S. Lukman, A. J. Musser, K. Chen, S. Athanasopoulos, C. K. Yong, Z. Zeng, Q. Ye, C. Chi, J. M. Hodgkiss, J. Wu, R. H. Friend, and N. C. Greenham, "Tuneable singlet exciton fission and triplet-triplet annihilation in an orthogonal pentacene dimer," Adv. Funct. Mater. **25**, 5452–5461 (2015).

[49]M. B. Smith and J. Michl, "Recent advances in singlet fission," Annu. Rev. Phys. Chem. **64**, 361–386 (2013).

[50]N. Monahan and X.-Y. Zhu, "Charge transfer-mediated singlet fission," Annu. Rev. Phys. Chem. **66**, 601–618 (2015).

[51]D. Beljonne, H. Yamagata, J. L. Brédas, F. C. Spano, and Y. Olivier, "Charge-transfer excitations steer the Davydov splitting and mediate singlet exciton fission in pentacene," Phys. Rev. Lett. **110**, 226402 (2013).

[52]C. E. Miller, M. R. Wasielewski, and G. C. Schatz, "Modeling singlet fission in rylene and diketopyrrolopyrrole derivatives: The role of the charge transfer state in superexchange and excimer formation," J. Phys. Chem. C **121**, 10345–10350 (2017).